GENETIC QUANTUM MEASUREMENTS
EMPIR-17FUN06 "SIQUST" Deliverable
D5: "Paper on genetic quantum measurement: a novel measurement approach"

S. Virzì, E. Rebufello, F. Piacentini, A. Avella, M. Gramegna, I. P. Degiovanni, M. Genovese
INRIM, Strada delle Cacce 91, I-10135 Torino, Italy
(Dated: December 10, 2020)

Genetic Quantum Measurements can be defined as a measurement protocol exploiting a genetic-like approach to significantly surpass the performances of traditional quantum projective measurements. Genetic Quantum Measurements are based on a sequence of steps consisting of an interaction-interference followed by a selective measurement. Interaction-interference essentially couples the observable of interest to a pointer observable, providing indirect estimation of the observable of interest. This estimation, for a reasonable number of interactions and for specific interaction strength, is expected to outperform, in terms of uncertainty reduction, the conventional projector-based quantum measurements (even when these last ones are considered optimal). Because of these performances, Genetic Quantum Measurement approach appears to be a disruptive technique that may lead to a general paradigm shift in quantum measurement. This is of utmost interest for all the quantum technologies, in general, and for quantum metrology and quantum-enhanced measurement, in particular.

I. INTRODUCTION

In computer science, a genetic algorithm involves mechanisms inspired by the process of natural selection. Genetic algorithms are commonly used to generate high-quality solutions to optimization and search problems by relying on bio-inspired operators such as mutation, crossover and selection[1].

In quantum mechanics the measurement procedure, following the von Neumann scheme[2], is described as a sequence composed of particle state preparation, interaction (described by a unitary operator) between quantum system and measuring device, and particle detection (typically described with the projective measurements formalism). Since the measurement induces the wavefunction collapse[3–6] in one of the eigenstates of the measurement basis, it is necessary to detect a statistically significant amount of particles to obtain a faithful estimate of the measured observable of interest. In this paper, we present and discuss a novel measurement concept we have devised: the Genetic Quantum Measurement.

Genetic quantum measurements (GQMs) represent a paradigm shift in the quantum measurement framework, since they use genetic-like approach to significantly surpass the performances of the conventional (projector-based) quantum measurement techniques. Indeed, GQMs, after the usual initial state preparation, take advantage of a repeated sequence of interaction and recombination leading to quantum interferences (here taking the role of the crossover in genetic processes) and selective measurements (corresponding to the genetic selection pressure). The quantum mechanical Superposition Principle, at the heart of the quantum parallelism advantage exploited in several of the forthcoming quantum technologies such as, e.g., quantum computers, plays the role of mutation, necessary to explore different evolution paths. Thanks to the quantum parallelism feature in the GQM approach all the possible "evolution trajectories" are explored at the same time.

A little bit more in detail: GQMs, after the initial state preparation consisting of filtering/selecting the particles in the chosen quantum state, are composed of a sequence of K steps each one with an interaction-interference followed by a selective measurement (i.e. a filtering procedure, ideally identical to the one exploited in the state preparation procedure). The interaction-interference is realized by coupling the observable of interest with another observable (the pointer, belonging to the measurement device Hilbert space) that will be used to perform the indirect measurement of the observable of interest. In none of the steps the detection of the quantum system is performed: thus, the same individual quantum system -provided that it survives after the selection process- at the end of the whole sequence of "interaction-interference plus selection" steps is detected measuring the value of the Pointer (or a related observable as, e.g., the observable canonically-conjugated to the Pointer). We will show that this procedure provides the (indirect) estimation of the observable of interest with an uncertainty substantially reduced with respect to the one achievable with the usual quantum measurement approach based on a prepare-and-measure scheme, when the same initial resources, i.e. the number of individual quantum systems, are considered.

In most of the cases, the prepare-and-measure approach saturates the quantum Cramer-Rao Bound, i.e. it represents the optimal quantum measurement, providing the minimum uncertainty achievable. Thus, at a first glance, it appears impossible that GQMs would be able to outperform what is expected to be the optimal quantum measurement. With a closer look, we will show that this advantage stems from the fact that the GQM approach takes advantage, during

the whole measurement process, of the selective measurement, strictly connected with the preparation stage. This additional information coming from the preparation/selection mechanism is assumed to be unavailable in the typical prepare-and-measure approach, as well as in the more general case of optimal quantum measurements (i.e. the ones saturating the quantum Cramer-Rao bound). This essentially explains why GQMs are able to provide such astonishing performances in terms of quantum uncertainty reduction. In this sense, GQMs appear to be useful to test unknown state preparations rather than unknown quantum state, since GQMs rely on the state-selective measurements that are assumed to be identical to the initial state preparation.

Because of these performances, GQMs appear to be a major advance in several fields where quantum measurements are involved, among all quantum technologies and specially in quantum metrology, where it may represent a disruptive breakthrough, because of its heavy uncertainty reduction feature. GQMs present some analogies, but also relevant differences, with respect to a couple of well established theoretical measurement paradigms, namely sequential measurements[7] and protective measurements[8–19].

Specifically, sequential measurements, analogously to GQMs, exploit a sequence of interactions, but without introducing the selective pressure (the selectiion measurements in GQMs) and with the aim of estimating a parameter of the interaction rather than a quantum observable. For this reason, sequential measurements do not take advantage of an ancillary Hilbert space (the one of the Pointer observable in the GQMs case). Furthermore, this theoretical idea assumes to be able to obtain some data/information after each interaction without detecting the individual quantum system undergoing it (i.e. without inducing the wave function collapse), a very challenging experimental task. On the contrary, the GQM approach extracts the information on the expectation value of the observable of interest only at the final detection stage: much more reasonable from the experimentalist's point of view.

The protective measurements concept is somehow analogous to the one of GQMs, since it takes advantage of a continuous protection of the quantum state (through a potential, or a quantum-Zeno-like projective measurement[20–27]) that is connected with an asymptotically infinite sequence of extremely weak interactions. In analogy with GQMs, the observable of interest estimation is obtained by an indirect measurement involving coupling with the expectation value of a pointer observable in an ancillary Hilbert space. The main concept behind protective measurement is that the estimation of the expectation value of the observable of interest is performed by the detection of a SINGLE quantum system. This is possible, from a theoretical point of view, since at each step the interaction is so weak that the probability of losing a photon, through the potential barrier or because of the state-projection, is negligibly small even after an infinite amount of such interaction-protection (projection) steps (something similar to what happens in the quantum Zeno effect). Obviously, it is experimentally impossible to have the full control of an infinitely weak interaction strength, and, at the same time, to realize something even only approximating an infinite amount of interaction-protection steps. GQM approach considers a finite amount of "interaction/interference plus selection" stages (ranging from few units to hundreds, or even thousands) and investigates any interaction intensity, from weak to strong, in order to optimize the trade-off between quantum system survival probability and uncertainty reduction. One of the most surprising features we will show is that GQMs a substantial advantage with respect to the Quantum-Cramer-Rao bound even when strong interaction is exploited. Furthermore we will show that the interaction strength, leading to the maximum advantage with respect to the Quantum-Cramer-Rao bound, depends on the number of steps of the GQM procedure. In some sense, it can be considered as a practical and (astonishingly) useful version of the ideal concept of protective measurement.

II. THEORETICAL MODEL

In the following we will describe the theory behind GQMs. Despite the fact that we discuss the case of our quantum optical experiment where we extract the expectation value of the photon polarisation $P = |H\rangle\langle H| - |V\rangle\langle V|$ by means of a measurement performed on a single detected photon, where H and V are the horizontal and vertical polarisations, our argument is completely general; indeed, we underline that, with minimal variation, it can be extended to observables having either discrete or continuous eigenvalues spectrum.

As explained above, to perform the GQM we need to couple P to take advantage of a pointer observable. In our experiment we take advantage of a spatial resolving detector, thus it is quite obvious to consider the space and polarisation degrees of freedom when we describe the wavefunction of our single photon, i.e. $|\Psi_{\text{in}}\rangle = |\psi_\theta\rangle \otimes |f_x\rangle$ with $|\psi_\theta\rangle = \cos\theta|H\rangle + \sin\theta|V\rangle$ and $|f_x\rangle = \int \mathrm{d}x\ f(x)|x\rangle$ where $f(x)$ is a Gaussian curve whose square is normalised to one, namely $f(x) = (2\pi\sigma^2)^{-\frac{1}{4}} \exp(-\frac{x^2}{4\sigma^2})$.

The GQM consists of a sequence of identical interactions, exploiting the spatial walk-off in non-linear crystals (using a technique completely analogous to the one used in, e.g.,[28]) corresponding to the unitary transformation $U = \exp(-ig\Pi_H \otimes \mathbf{P})$ (being $\mathbf{P}$ the transverse momentum operator along the x axis, and g the von Neumann coupling constant between $\mathbf{P}$ and the projector $\Pi_H = |H\rangle\langle H|$), and the selection measurement, performed by exploiting the polarisation projector $\Pi_\theta = |\psi_\theta\rangle\langle\psi_\theta|$. Actually, this can be also described as a test on an unknown state preparation

procedure exploiting a series of identical projective measurements, the first one really used to prepare (select) the single-photon state, while the other ones used as filtering measurements. After K steps of this sequence consisting of a interaction followed by a filtering measurement (selection), the non-normalised output state of the single photons will be:

$$|\Psi_{\rm out}\rangle = (\Pi_\theta U)^K |\Psi_{\rm in}\rangle = \left(\langle H|\Pi_\theta|H\rangle e^{-ig\mathbf{P}} + \langle V|\Pi_\theta|V\rangle \mathbf{1}_x\right)^K |\Psi_{\rm in}\rangle. \quad (1)$$

Thus, the probability that the single-photon survives after K interaction-selection steps is $p_{\rm sur}(K) = {\rm Tr}[|\Psi_{\rm out}\rangle\langle\Psi_{\rm out}|]$, while the probability of finding the detected single-photon in a specific position x_0 of our spatial-resolving detector (given that it survived the verification process) is

$$\begin{aligned} F_K(x_0) &= p_{\rm sur}(K)^{-1}\ {\rm Tr}[|x_0\rangle\langle x_0|\Psi_{\rm out}\rangle\langle\Psi_{\rm out}|] \\ &= p_{\rm sur}(K)^{-1}\ \left(\sum_{n=0}^{K} \frac{K!}{n!(K-n)!}\langle H|\Pi_\theta|H\rangle^n \langle V|\Pi_\theta|V\rangle^{K-n} f(x_0+ng)\right)^2. \end{aligned} \quad (2)$$

As explained, the spatially-resolved detection of the single-photon provides an estimation of the value of P. A crucial question is related to the quality of this estimation, i.e. the uncertainty that can be associated with this estimation. This uncertainty is obviously associated with the uncertainty on the arrival position x of each detected single photon, related to the probability distribution profile $F_K(x)$. The uncertainty in the position is $u(x) = \sqrt{\epsilon(x^2) - \epsilon(x)^2}$, with $\epsilon(x^n) = \int {\rm d}x\ x^n F_K(x)$. Then, we note that there ia a correspondence between the value of $\langle P\rangle$ and the average position $\epsilon(x)$: the H-polarisation ($\langle P\rangle = 1$) corresponds to the position $\epsilon(x) = \frac{Kg}{2}$, while the V-polarisation ($\langle P\rangle = -1$) corresponds to the position $\epsilon(x) = -\frac{Kg}{2}$ (actually, the V-polarisation is not affected by the interaction according to the unitary interaction operator U, while the H-polarisation is shifted by Kg, because of the fact that each interaction induces a shift g, according to Eq. (2). Anyway, we decided to shift the whole X axis by $-\frac{Kg}{2}$ for an easier comparison with the well-known Stern-Gerlach experiment). Thus, the uncertainty on $\langle P\rangle$ associated with the detection of a single photon can be obtained simply by re-scaling the spatial uncertainty $u(x)$, i.e. $u(P) = u(x)\ \frac{2}{Kg}$.

III. BEATING THE QUANTUM-CRAMER-RAO BOUND

It is interesting to compare the performance of the GQM technique presented above in situations of strong and weak interaction, corresponding to $g \gg \sigma$ and $g \ll \sigma$ respectively, versus the usual technique involving a single projective measurement, for example exploiting a polarizing-beam-splitter (PBS). In the PBS measurement, starting from M initial photons in the polarisation state $|\psi\rangle$ the probability distribution of observing m photons V-polarised (and, obviously, $(M-m)$ H-polarised) is the binomial-one with probability parameter $(\cos\theta)^2$. Thus, the estimator of P is $P = \frac{2m}{M} - 1$ and the uncertainty on this estimator can be evaluated as $u_{\rm PBS}(P) = \sqrt{\langle P^2\rangle - \langle P\rangle^2} = \frac{|\sin(2\theta)|}{\sqrt{M}}$. This uncertainty level is easily demonstrated to be the optimal one in terms of quantum Fisher information (indeed the quantum Fisher Information is $\mathcal{H} = \sin(2\theta)^{-2}$), i.e. the one that saturates the quantum Cramer-Rao bound[29].

In order to provide a fair comparison between this PBS-based measurement and our GQM-based one we should consider the two measurement approaches exploiting the same initial resources, i.e. the same number of initially prepared photons. In the GQM case we have considered the uncertainty associated with the detection of a single-photon, but the probability of survival to a K-step GQM process is $p_{\rm sur}(K)$, meaning that to have one photon detected at the end of the GQM we need, on average, $1/p_{\rm sur}(K)$ initial photons. To perform a fair comparison, we set $M = 1/p_{\rm sur}(K)$ also in the PBS measurement case, and we define the ratio $R = \frac{u_{\rm PBS}(P)}{u(P)}$.

This is what we show in Fig. 1, where we plot the ratio $R = \frac{u_{\rm PBS}(P)}{u(P)}$ between the uncertainties on $\langle P\rangle$ achievable with the two measurement approaches ($u(P)$ and $u_{\rm PBS}(P)$ respectively, considering $u_{\rm PBS}(P)$ the uncertainty associated with the measurement procedure saturating the Quantum Cramer-Rao bound, i.e. being equal to the inverse of the square root of the Quantum Fisher information[29]). R is plotted versus the interaction strength $\xi = g/\sigma$ and the horizontal polarisation component of the single-photon state $|\psi\rangle$ (specifically, $(\cos\theta)^2$ is $\langle\psi|\Pi_H|\psi\rangle$). As we said, we consider in both cases the same initial resources (photon number), taking into account the photons lost along the GQM steps. We study two different scenarios: $K = 7$ (yellow surface) and $K = 100$ (blue surface). One immediately notices that, in both cases, GQM is almost always advantageous ($R > 1$) with respect to the projective measurement, going below the $R = 1$ plane (in magenta) only in presence of extremely weak interactions (it is evident from the figure, but, e.g., also for $K = 100$ and $g/\sigma = 0.02$ and $|\psi\rangle = 2^{-1/2}(|H\rangle + |V\rangle)$ we have $R = 0.996$). In our experiment, with $\xi \sim 0.4$ and just $K = 7$, a 10% advantage is already present for most of the possible states, even if the maximum for R corresponds to $\xi \sim 1$. For $K = 100$, instead, the reasonably weak interaction $\xi \sim 0.4$ grants the maximum of

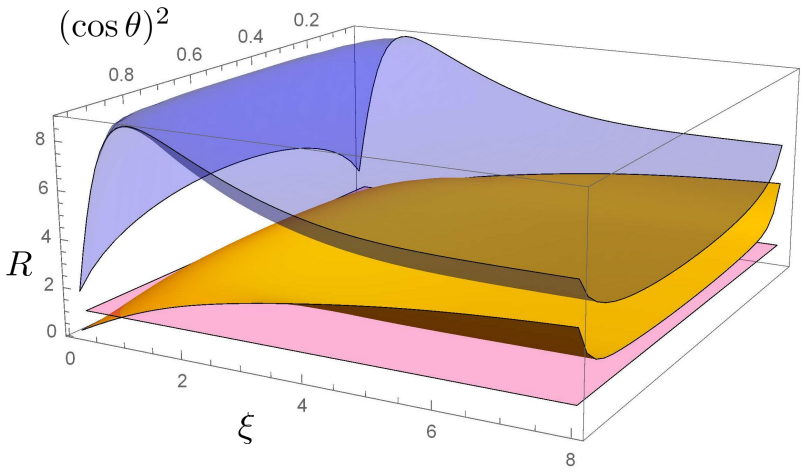

FIG. 1: Yellow surface: ratio $R = \frac{u_{\rm PBS}(P)}{u(P)}$ for a GQM scheme with $K = 7$ interaction-selection stages (as in our experiment), plotted versus the interaction strength ξ and the H-polarisation component $(\cos\theta)^2$ of the single-photon state $|\psi\rangle$. Blue surface: ratio R for a GQM with $K = 100$ stages. Magenta surface: $R = 1$ bound, discriminating the part where GQM approach is advantageous (above) and disadvantageous (below) with respect to the projective measurement.

the advantage ($R > 8.5$ almost everywhere), while for stronger interaction the advantage is reduced to $R < 4$. The advantage of the GQM technique comes from the very high survival probability of the single photons. This comes from the fact that, in presence of a sequence of identical interaction-selection stages as in our scheme, the relative probability of losing a photon in a selection process decreases with the single photon advancing in the sequence, since it is more likely to find the photon close to the "right paths" created in previous steps.

Here we want to stress that, even though projective measurement is an optimal measurement for the parameter P, i.e. a measurement procedure able to reach the quantum Cramer-Rao bound[29], GQMs allow obtaining an estimation of $\langle P\rangle$ far better than the one achievable with such method, surpassing this way the quantum Cramer-Rao bound itself. R can be understood also as a parameter identifying the resources needed to achieve the same level of uncertainties in the two measurement techniques: in fact, to achieve the same level of uncertainty, the initial number of photons needed in the PBS measurement is the one used for the GQM multiplied by a factor R^2.

The advantage of the GQM technique comes from the very high survival probability of the selected photons. As evident from Fig. 2 (a), indeed, with $K = 100$ interactions and $g/\sigma \sim 0.4$ we have $p_{\rm sur} > 0.57$ even for the most lossy state. Also in the case of strong interaction $g/\sigma = 6$ the survival probability is surprisingly high ($p_{\rm sur} > 0.05$).

To understand this, one should consider the situation in which the GQM is performed with strong interactions such that the shift due to each crystal will be much larger than the width of the beam (the situation depicted in Fig. 3). Then, the readings of the detector provide the expectation value with a precision scaling as $1/\sqrt{K}$, reminding the one of the projective measurement, where the uncertainty scales of a factor $1/\sqrt{N}$ with the number N of exploited photons.

The advantage can be further appreciated observing the fact that the average number of photons needed for observing a single photon outgoing the GQM, i.e. $1/p_{\rm sur}(K)$, grows at a much slower pace with respect to K, as shown in Fig. 2 (b). This comes from the fact that, in presence of a sequence of identical interaction-selection stages as in our scheme, the relative probability of losing a photon in a selection step because of unsuccessful selection process decreases with the single photon advancing in the sequence since photons are more likely on the "right path" (see Fig. 3).

IV. PROOF-OF-PRINCIPLE EXPERIMENT

Our experimental setup (Fig. 4) is essentially composed of three parts. The first part (launcher and state preparation/selection) produces single photons in well-defined linear polarisation states, by means of a heralded single-photon source (SPS)[30] based on Type-I Spontaneous Parametric Down-Conversion (SPDC). In the second part (genetic evolution) we have created $K = 7$ steps of interaction and selection, implemented by means of birefreingent crystals and polarisation filters, respectively. Finally, in the third part (detection) the photons are detected by a camera

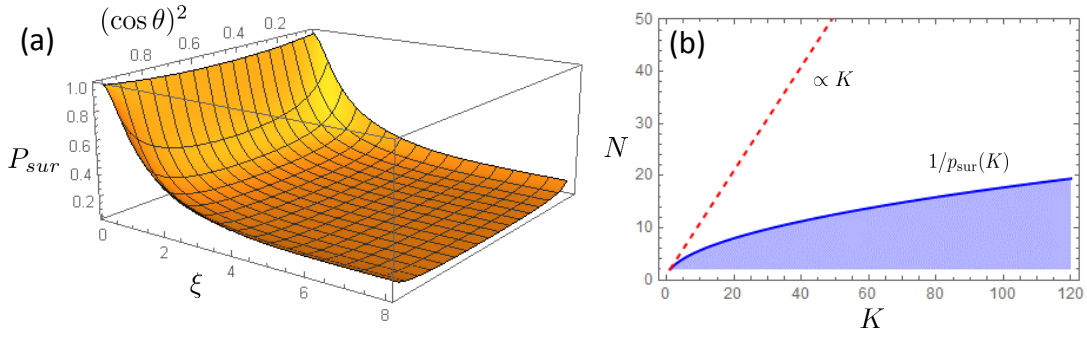

FIG. 2: Plot (a): GQM photon survival probability $p_{\rm sur}(K = 100)$ (a) plotted versus $\xi = g/\sigma$ (representing the interaction strength) and $(\cos\theta)^2$ (i.e. the H-polarisation component) of the single-photon state $|\psi\rangle$. Plot (b): the shaded area represents the average number N of initial photons needed to observe a photon at the end of the GQM process $(1/p_{\rm sur}(K))$ versus the number of interaction-selection stages K (the worst-case scenario, indicated by the blue curve on the boundary, corresponds to the state $|\psi_{\frac{\pi}{4}}\rangle$). For comparison, a dashed line corresponding to the linear scaling with K is reported.

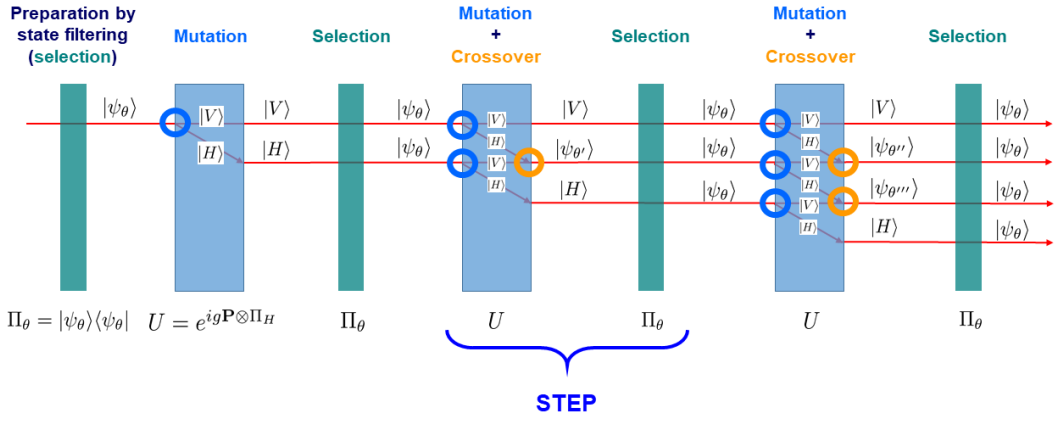

FIG. 3: GQM scheme in case of strong interaction $g/\sigma >> 1$. here, the red lines represent the photon trajectories, with the H- and V-polarisation completely separated by the birefringent crystals. From the second birefringent crystal onwards, the H- and V-paths recombine in some spots (indicated by the orange circle) in a coherent way, forming a state with non-zero survival probability in the subsequent selection stage. This effect results in a reduction of photon losses, specially in the paths close to the expectation value of $\langle P\rangle$, granting advantage to the GQMs scheme with respect to the projective one . This can be intuitively understood analysing the probability distribution of the survived photons considering, e.g. $|\psi_\theta\rangle = (|H\rangle + |V\rangle)/\sqrt{2}$.

which consists of an array of single-photon detectors. The SPS is based on a 796 nm mode-locked Ti:Sapphire laser (repetition rate: 76 MHz), whose second harmonic emission pumps a $10 \times 10 \times 5$ mm $LiIO_3$ non-linear crystal, in which correlated photons are produced by SPDC. The idler photons ($\lambda_i = 920$ nm) are coupled to a single-mode fiber (SMF) and then addressed to a Silicon Single-Photon Avalanche Diode operated in Geiger mode (SPAD), heralding the presence of the correlated signal photons ($\lambda_s = 702$ nm). These, after being SMF-coupled, are addressed to a launcher injecting them into the free-space optical path, where the GQM protocol is implemented. After the launcher, the heralded single photons are collimated by a telescopic system, and then prepared in the linear polarisation state $|\psi_\theta\rangle$ (by means of a calcite polariser followed by a half-wave plate). We exploited the flexibility of the telescopic system to obtain the single-photon collimated spatial distributions of different widths (specifically, we observe beam widths of 2.14 ± 0.02, 2.93 ± 0.03 and 3.998 ± 0.004 pixels of the SPAD array, corresponding to the three interaction

strength $\xi = 0.79 \pm 0.01$, 0.56 ± 0.01 and 0.415 ± 0.003). We have estimated the quality of our single-photon emission with a Hanbury-Brown and Twiss interferometer, obtaining a value for the parameter α[31] (directly connected to the second-order Glauber autocorrelation function $g^{(2)}$) of 0.13 ± 0.01 without any background or dark count subtraction, that being largely below 1 testifies the goodness of our single photon source. The interaction steps of the genetic evolution couple quantum degrees of freedom of the single photon exploiting birefringence. In our optical path we can insert up to $K = 7$ birefringent units, each of them composed of two different calcite crystals (the number $K = 7$ of verification measurements was chosen from practical considerations approximating the ideal case of large K; because of losses originating from optical elements imperfections, further increasing K would result in a low photon survival probability).

The first crystal of each element is a 2 mm long birefringent crystal whose extraordinary (e) optical axis lies in the $X - Z$ plane, with an angle of $\pi/4$ with respect to the Z direction. Due to the spatial walk-off effect experienced by the horizontally-polarised photons (along the Y direction), horizontal and vertical-polarisation paths get slightly separated (coupling to the pointer variable). The second crystal of each unit is a 1.1 mm long birefringent crystal with the optical e-axis along the Y axis (thus not contributing to the transversal walk-off) that nullifies, through phase compensation, the temporal walk-off introduced by the first one. The selection of the quantum state is realised by inserting a thin-film polariser after each birefringent unit, projecting the photons onto the same polarisation of the initial state $|\psi_\theta\rangle$. At the end of the optical path, the photons are detected by a spatial-resolving single-photon detector prototype. This device is a two-dimensional array made of 32×32 "smart pixels" - each one hosting a SPAD-based single-photon detector and its front-end electronics[32]. The SPAD array is gated with a 6 ns integration windows, triggered by the SPAD in the heralding arm in order to reduce the dark counts and improve the signal-to-noise ratio.

We tested the setup with three different states, namely, $|\psi_{\frac{17\pi}{60}}\rangle = 0.629|H\rangle + 0.777|V\rangle$, $|\psi_{\frac{\pi}{4}}\rangle = \frac{1}{\sqrt{2}}(|H\rangle + |V\rangle)$, $|\psi_{\frac{\pi}{8}}\rangle = 0.924|H\rangle + 0.383|V\rangle$ and, as already explained, with the three different interaction strengths mentioned above. The obtained results are summarized in Fig. 5.

By removing the selection filters (i.e. realising the projective measurement case) the photon counts accumulate around the positions $x = \pm a$, forming the distributions reported in panels (a), (b) and (c) for the states $|\psi_{\frac{\pi}{4}}\rangle$, $|\psi_{\frac{17\pi}{60}}\rangle$ and $|\psi_{\frac{\pi}{8}}\rangle$, respectively. From these photon-counts distributions, we can evaluate, for each state, the polarisation expectation value, obtaining $\langle P_{\frac{\pi}{4}}\rangle = -0.03(4)$, $\langle P_{\frac{17\pi}{60}}\rangle = -0.21(2)$, $\langle P_{\frac{\pi}{8}}\rangle = 0.72(2)$, all in excellent agreement with the theoretical expectations ($\langle P_{\frac{\pi}{4}}\rangle = 0$, $\langle P_{\frac{17\pi}{60}}\rangle = -0.208$ and $\langle P_{\frac{\pi}{8}}\rangle = 0.707$, respectively).

The expectations values obtained in the case of GQMs are respectively $\langle P_{\frac{\pi}{4}}\rangle = -0.012(14)$, $\langle P_{\frac{17\pi}{60}}\rangle = -0.19(2)$ and $\langle P_{\frac{\pi}{8}}\rangle = 0.72(2)$, in good agreement with the theory as well as with the ones obtained without selective measurement the single photons. In order to obtain these values, the dark counts of the 32×32 SPAD array, responsible for the

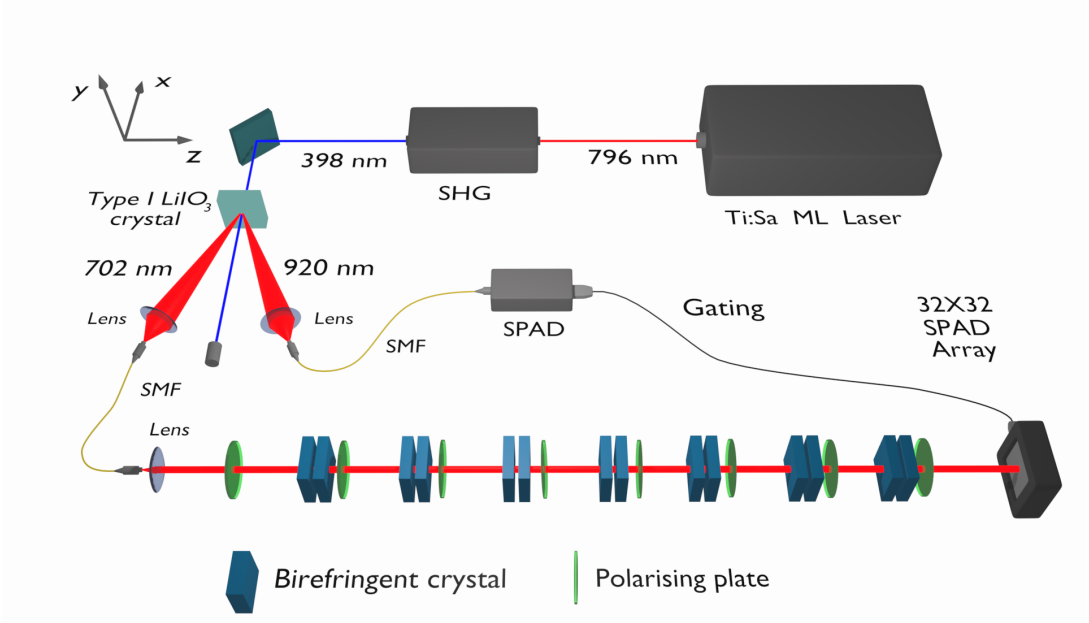

FIG. 4: Experimental setup.

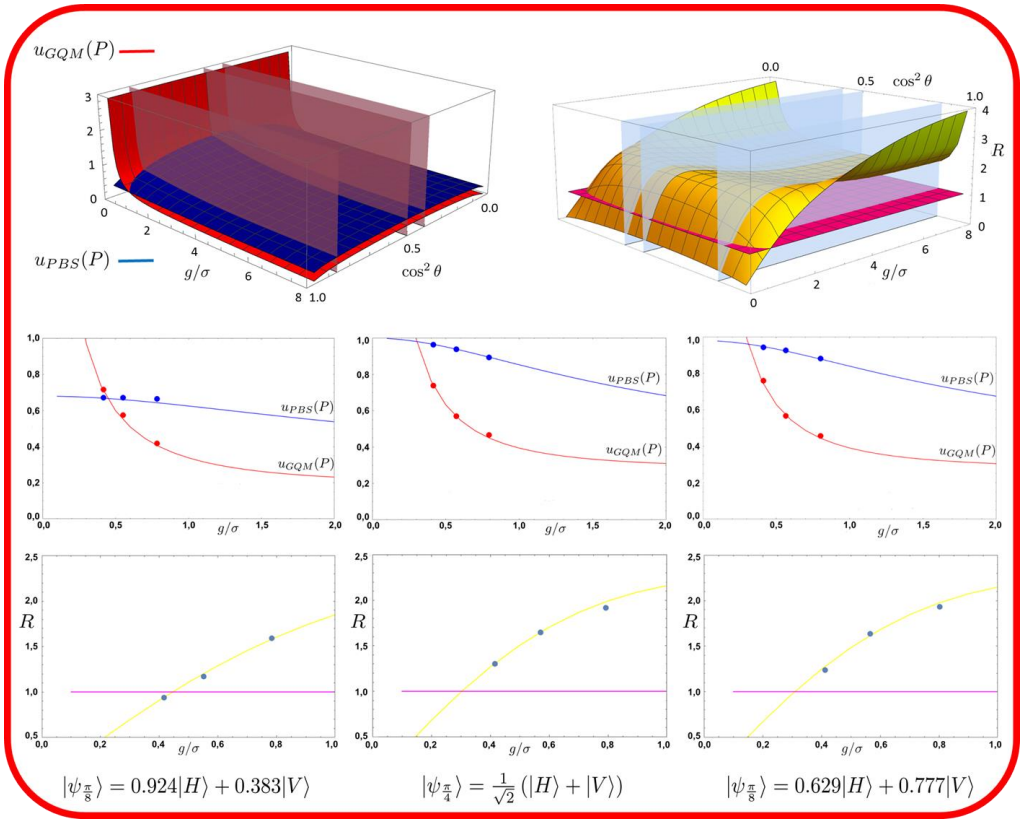

FIG. 5: Left upper plot: the theoretical uncertainties associated with $\langle P\rangle$ in a projective measurement (blue surface) and a GQM (red surface), considering $M = p_{sur}^{-1}$ identically-prepared initial photons, with respect to the GQM interaction strength g/σ and the H-polarization component. Vertical cuts are made in correspondence of the three polarisation states realised in the experiment. Right upper plot: ratio $R = \frac{u_{PBS}(P)}{u(P)}$ (yellow surface), again with vertical cuts in correspodence of the chosen polarisation states. The magenta plane shows the $R = 1$ threshold, above which GQM outperforms traditional projective measurements. Middle plots: uncertainties related to the PBS measurement (in blue) and GQM (in red) in correspondence of the three cuts of the upper left plot, i.e. for the three states under investigation. The curves represent the theoretical expectations, while the dots indicate the experimental results. Bottom line plots: cuts of the R surface (yellow curves, with the magenta lines indicating the $R = 1$ plane) in correspondence of the examined polarisation states, with the R experimental values reported as blue dots.

"floor" of counts in all the six plots, were properly evaluated and subtracted.

Fig. 5 shows a comparison between the theoretical and experimental uncertainties given by the two measurement protocols, considering for the GQM $K = 7$. The left upper plot hosts the theoretical uncertainties associated with $\langle P\rangle$ in a projective measurement (blue surface) and a GQM (red surface), considering $M = p_{sur}^{-1}$ identically-prepared initial photons, with respect to the GQM interaction strength g/σ and the H-polarization component. The vertical cuts highlight the three polarisation states realised in the experiment. The right upper plot, instead, shows the ratio R between the two quantities shown in the left plot, again with vertical cuts in correspodence of the chosen polarisation states. The three middle plots show the PBS measurement (in blue) and GQM (in red) uncertainties in correspondence of the three cuts uf the upper left plot, i.e. for the three states under investigation. The curves represent the theoretical expectations, while the dots indicate the experimental results. Aside of the immediately visible very good agreement between theory and experiment, one can appreciate how GQM always outperforms the projective measurement, with the sole exception of the $\xi = 0.415 \pm 0.003$ experiment with $|\psi_{\frac{\pi}{8}}\rangle$, for which the GQM interaction intensity was too weak to provide an adequate resolution for estimating $\langle P\rangle$ with sufficient precision. Finally, in the bottom line plots the corresponding cuts of the R surface are shown (yellow curves, with the magenta lines indicating the $R = 1$ plane above which GQM results advantageous), with the R experimental values superimposed as blue dots. Here it is evident how, with the exception of the aforementioned case, the GQM approach outperforms the PBS one, gaining even a factor of 2 in terms of uncertainty reduction with just $K = 7$: this is a clear hint of the huge potential impact of GQM in quantum metrology and sensing, as well as its relevance for other quantum technologies.

Obviously, the above considerations assume an ideal scenario where the only source of losses in the GQMs is represented by the projection measurement preforming the selection of the state, neglecting completely the optical losses induced by the real optical devices present in the experimental setup. In the specific case of our experiment, the optical losses greatly reduce the advantage discussed so far, but this is a technical limitation that can be, in principle, strongly reduced. It is important to underline that the advantage of the GQM technique can become absolutely relevant in a less lossy measurement scenario, and that our proof-of-principle experiment and simulations pave the way to the exploitation of the GQM approach in atomic or solid state quantum systems, where losses are typically lower than the ones experienced in photon-based experiments.

V. CONCLUSION

In conclusion, we have showed both theoretically and experimentally that GQMs represent a real paradigm shift: taking advantage of a genetic-like approach to significantly surpass the performances of the conventional projector-based quantum measurement techniques. GQMs exploit a sequence of K stages implementing an interaction-recombination paired with a selective measurement The effect of the interaction-interference event consists in coupling the observable of interest with another observable that will be used to perform the indirect measurement of the observable of interest, as in the case of the von Neumann measurement, but repeated several times before detecting the quantum system.

This indirect estimation of the observable of interest is obtained with an uncertainty substantially reduced with respect to the one achievable with the usual projective measurement approach when the same initial resources, i.e. the number of initial individual quantum systems, are considered. As explained, GQMs are useful to test unknown state preparation systems rather than unknown quantum state, since GQMs exploit, during the measurement process, the state-selective measurements equivalent to the initial state preparation.

Because of these astonishing performances, GQMs appear to be a disruptive technique that may lead to a general paradigm shift in quantum measurement. They are of utmost interest not only for studies on quantum metrology and quantum-enhanced measurement, but also for all the quantum technologies, specifically when the creation of multiple copies of the quantum system of interest is challenging from some peculiar point of view, e.g. economical, technological, etc.

Acknowledgments

This work has been supported by EMPIR-17FUN06 “SIQUST” (the EMPIR initiative is co-funded by the EU H2020 and the EMPIR Participating States).

[1] M. Mitchell (1996). An Introduction to Genetic Algorithms. Cambridge, MA: MIT Press.
[2] W. H. Zurek, Decoherence, einselection, and the quantum origins of the classical, Reviews of Modern Physics 75, 715 (2003).
[3] M. F. Pusey, J. Barrett, T. Rudolph, On the reality of the quantum state. *Nat. Phys.* **8**, 475-478 (2012).
[4] L. Hardy, Are quantum states real? *Int. J. Mod. Phys. B* **27**, 1345012 (2013).
[5] M. Ringbauer, B. Duffus, C. Branciard, E. G. Cavalcanti, A. G. White, A. Fedrizzi, Measurements on the reality of the wavefunction. *Nat. Phys.* **11**, 249-254 (2015).
[6] M. Genovese, Interpretations of Quantum Mechanics and the measurement problem. *Adv. Sci. Lett.* 3, 249 (2010).
[7] See e.g. D. Bugarth et al., Quantum Estimation with Sequential Measurements, New J. Phys. 17, 113055 (2015), and Ref.s therein
[8] Y. Aharonov, L. Vaidman, Measurement of the Schrödinger Wave of a Single Particle. *Phys. Lett. A* **178**, 38 (1993).
[9] C. Rovelli, Comment on “Meaning of the wave function”. *Phys. Rev. A* **50**, 2788 (1994).
[10] W. G. Unruh, Reality and measurement of the wave function. *Phys. Rev. A* **50**, 882 (1994).
[11] G. M. D’Ariano, H. P. Yuen, Impossibility of measuring the wave function of a single quantum system. *Phys. Rev. Lett.* **76**, 2832 (1996).
[12] Y. Aharonov, J. Anandan, L. Vaidman, The Meaning of Protective Measurements. *Found. Phys.* **26**, 117-126 (1996).
[13] N. H. Dass, T. Qureshi, Critique of protective measurements. *Phys. Rev. A* **59**, 2590 (1999).
[14] J. Uffink, How to protect the interpretation of the wave function against protective measurements. *Phys. Rev. A* **60**, 3474 (1999).
[15] S. Gao, Protective Measurement and Quantum Reality (Cambridge University Press, UK, 2015).
[16] Y. Aharonov, B. G. Englert, M. O. Scully, Protective measurements and Bohm trajectories. *Phys. Lett. A* **263**, 137 (1999).

[17] M. Schlosshauer, Measuring the quantum state of a single system with minimum state disturbance. *Phys. Rev. A* **93**, 012115 (2016).
[18] Y. Aharonov, L. Vaidman, Protective Measurements of Two-State Vectors. In *Potentiality, Entanglement and Passion-at-a-Distance*, eds/ R. S. Cohen, M. Horne and J. Stachel, BSPS 1-8, (Kluwer, 1997), quant-ph/9602009.
[19] F. Piacentini, A. Avella, E. Rebufello, R. Lussana, F. Villa, A. Tosi, M. Gramegna, G. Brida, E. Cohen, L. Vaidman, I. P. Degiovanni, M. Genovese, Determining the quantum expectation value by measuring a single photon, *Nature Phys.*, **13** 1191 (2017).
[20] B. Misra, E. C. G. Sudarshan, The Zeno's paradox in quantum theory. *J. Math. Phys.* **18**, 756 (1977).
[21] J. Dressel, M. Malik, F. M. Miatto, A. N.Jordan and R. W. Boyd, Understanding quantum weak values: Basics and applications. *Rev. Mod. phys.* **86**, 307 (2014).
[22] W. M. Itano, D. J. Heinzen, J. J. Bollinger, and D. J. Wineland, Quantum Zeno effect. *Phys. Rev. A* **41**, 2295 (1990).
[23] P. G. Kwiat, A. G. White, J. R. Mitchell, O. Nairz, G. Weihs, H. Weinfurter, A. Zeilinger, High-Efficiency Quantum Interrogation Measurements via the Quantum Zeno Effect. *Phys. Rev. Lett.* **83**, 4725 (1999).
[24] J. M. Raimond, C. Sayrin, S. Gleyzes, I. Dotsenko, M. Brune, S. Haroche, P. Facchi and S. Pascazio, Phase Space Tweezers for Tailoring Cavity Fields by Quantum Zeno Dynamics. *Phys. Rev. Lett.***105**, 213601 (2010).
[25] L. Bretheau, P. Campagne-Ibarcq, E. Flurin, F. Mallet, B. Huard, Quantum dynamics of an electromagnetic mode that cannot contain N photons. *Science* **348**, 776 (2015).
[26] A. Signoles, A. Facon, D. Grosso, I. Dotsenko, S. Haroche, J. Raimond, M. Brune, S. Gleyzes, Confined quantum Zeno dynamics of a watched atomic arrow. *Nat Phys.***10**, 715 (2014).
[27] G. Mazzucchi, W. Kozlowski, S. F. Caballero-Benitez, T. J. Elliott and I. B. Mekhov, Quantum measurement-induced dynamics of many-body ultracold bosonic and fermionic systems in optical lattices. *Phys. Rev. A* **93**, 023632 (2016).
[28] F. Piacentini, A. Avella, M. P. Levi, M. Gramegna, G. Brida, I.P. Degiovanni, E. Cohen, R. Lussana, F. Villa, A. Tosi, F. Zappa, and M. Genovese, Measuring Incompatible Observables by Exploiting Sequential Weak Values. *Phys. Rev. Lett.* **117**, 170402 (2016).
[29] M. G. A. Paris, Quantum Estimation For Quantum Technology. *Int. J. Quantum Inform.* **07**, 125 (2009).
[30] G. Brida, I. P. Degiovanni, M. Genovese, F. Piacentini, P. Traina, A. Della Frera, A. Tosi, A. Bahgat Shehata, C. Scarcella, A. Gulinatti, M. Ghioni, S. V. Polyakov, A. Migdall, A. Giudice, An extremely low-noise heralded single-photon source: A breakthrough for quantum technologies. *Applied Phys. Lett.* **101**, 221112 (2012) and ref.s therein.
[31] P. Grangier, G. Roger, A. Aspect, Experimental Evidence for a Photon Anticorrelation Effect on a Beam Splitter: A New Light on Single-Photon Interferences. *Eur. Phys. Lett.* **1**, 173 (1986).
[32] F. Villa, R. Lussana, D. Bronzi, S. Tisa, A. Tosi, F. Zappa, A. Dalla Mora, D. Contini, D. Durini, S. Weyers, W. Brockherde, CMOS Imager With 1024 SPADs and TDCs for Single-Photon Timing and 3-D Time-of-Flight. *IEEE J. Sel. Top. Quantum Electron.* **20**, 3804810 (2014).